Electronic Supplementary Material (ESI) for RSC Advances

Are Ionic Liquids Suitable Media for Boron Nitride Exfoliation and Dispersion? Insight *via* Molecular Dynamics Simulation

Ganesh Kamath and Gary A. Baker*

Department of Chemistry, University of Missouri-Columbia, Columbia, MO 65211

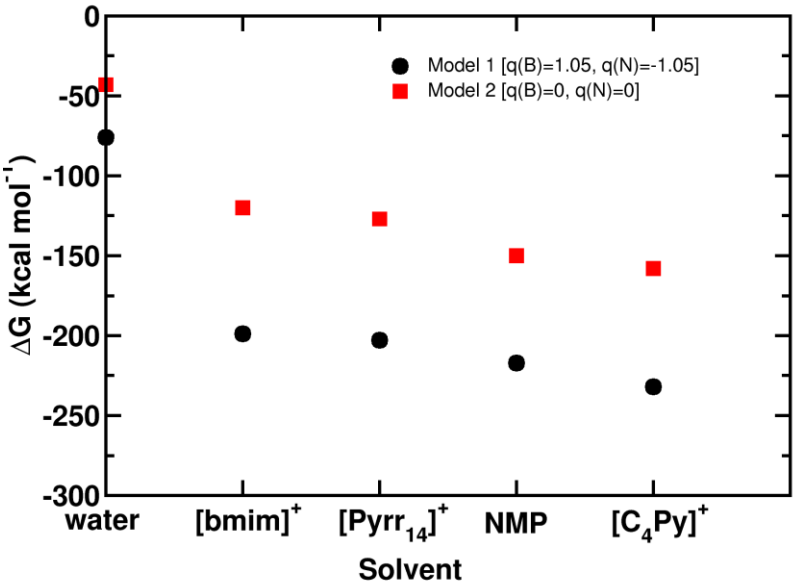

Fig. S1. ABF-calculated Gibbs free energies for exfoliation and dispersion of an h-BN monolayer from bilayered h-BN in water, NMP, and various ILs containing the $[NTf_2]^-$ anion.

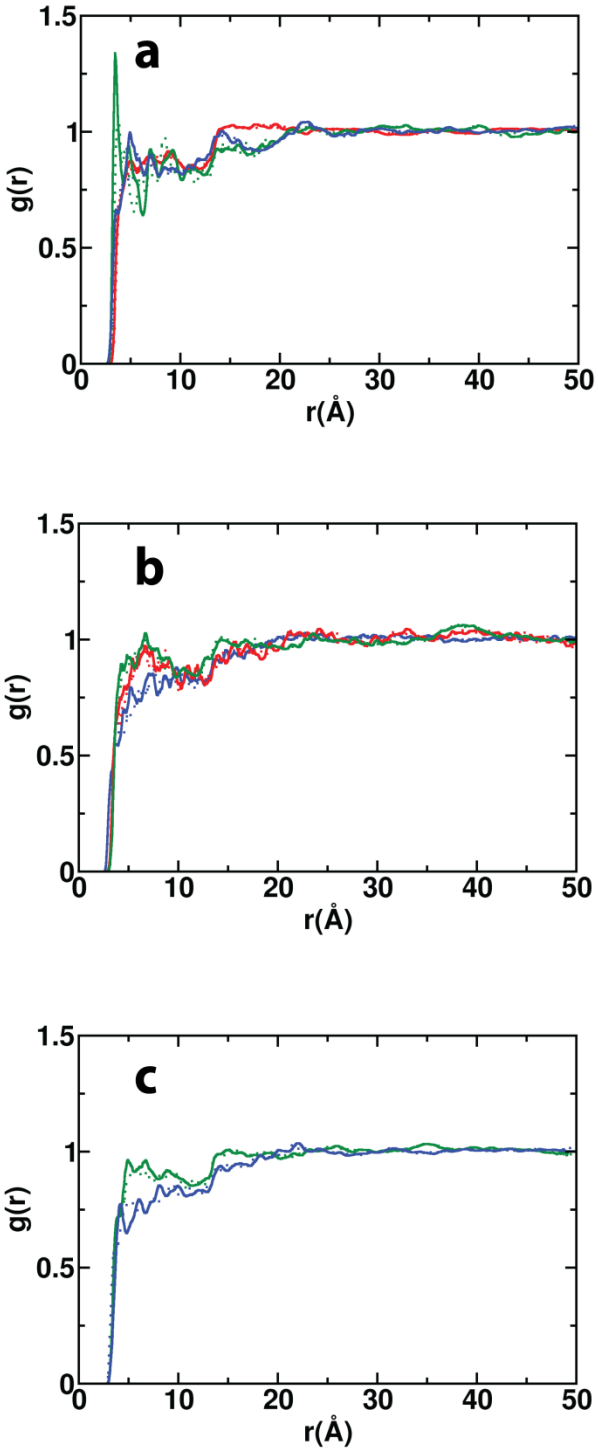

Fig. S2. IL cation interactions with h-BN (Model 1) for (a) [bmim][NTf_2] (b) [$Pyrr_{14}$][NTf_2], and (c) [C_4Py][NTf_2]. Solid curves show the RDFs of the methyl carbons (red curves), butyl chain (green curves), and ring (blue curves) with nitrogen (N) atoms of the h-BN surface. Dotted profiles give the corresponding RDFs for the methyl, butyl, and ring interactions with boron (B) of the h-BN surface.

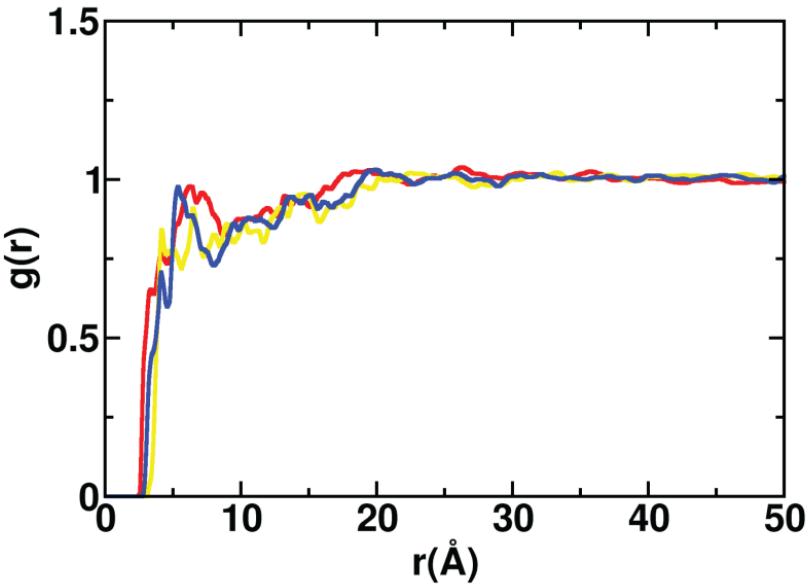

Fig. S3. $[NTf_2]^-$ anion interactions with h-BN (model 1) for the case of [bmim][NTf_2]. RDFs of the O (red curve), S (yellow curve), and N (blue) atoms of $[NTf_2]^-$ with the N atoms of h-BN are shown. The presence of weak peaks around 4.3 Å in all cases, with a more significant secondary solvation peak around 5.5 Å, suggests the presence of long-range electrostatics and conceivably anion–π interactions as well.

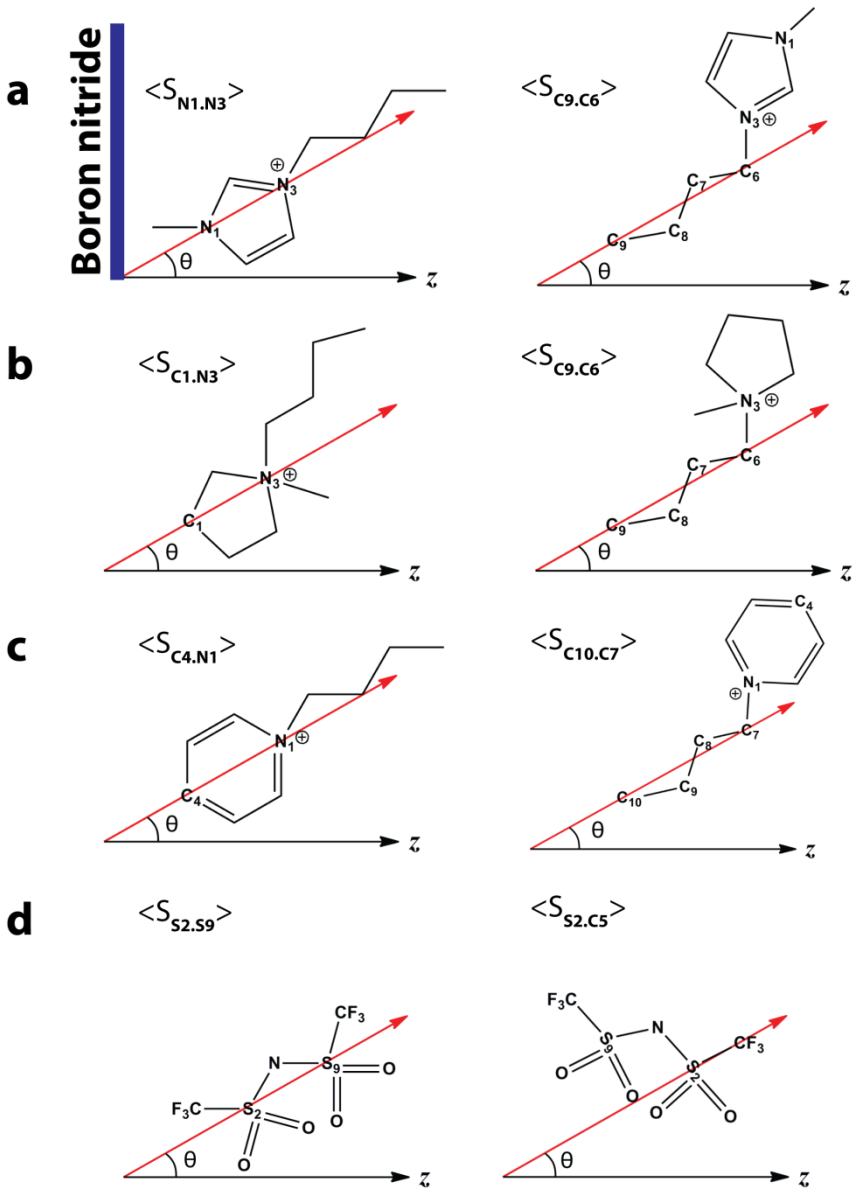

Fig. S4. Definition of the angle θ used to determine the orientation of the (a) $[bmim]^+$, (b) $[Pyrr_{14}]^+$, and (c) $[C_4Py]^+$ cations with respect to the *z* axis normal to the h-BN surface. The left panel gives the cation ring orientation with respect to the *z* axis normal to the h-BN surface while the panel on the right shows the definition for the orientation of the pendant butyl chains relative to the h-BN surface. The ordering parameter corresponding to θ is given by $\langle S \rangle = 1.5 \cos^2\theta - 0.5$. (d) Definition of the angle θ used to determine the orientation of the $[NTf_2]^-$ anion with respect to the *z* axis normal to the h-BN surface. (Left) The $S_2.S_9$ vector. (Right) The $S_2.C_5$ vector. This nomenclature conforms to the vector definition proposed by Lisal et al.[S1]

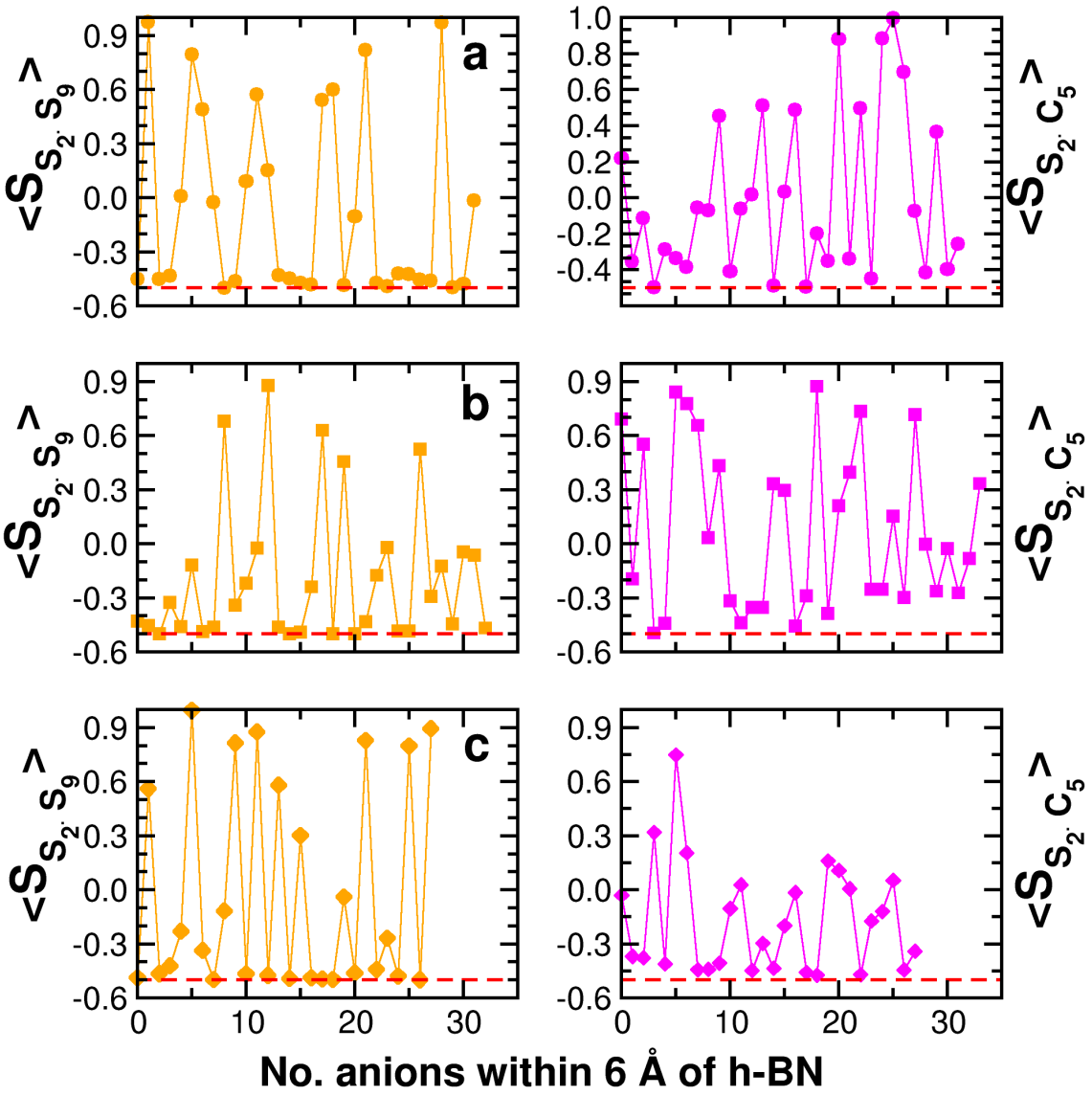

Fig. S5. (Left) The order parameter <S> defined by the $S_2.S_9$ vector of $[NTf_2]^-$ anions within 6 Å of the h-BN sheet (Model 1) for (a) [bmim][NTf_2], (b) [$Pyrr_{14}$][NTf_2], and (c) [C_4Py][NTf_2]. (Right) The corresponding <S> described along the $S_2.C_5$ vector of $[NTf_2]^-$. Remarkably, irrespective of the cation identity, more than 50% of the $[NTf_2]^-$ anions displayed an $S_2.S_9$ vector parallel to h-BN, analogous to the anion orientation at the air–liquid interface reported by Lisal et al.[S1] In comparison, the $S_2.C_5$ vector was distributed much more randomly relative to the h-BN plane. The $[NTf_2]^-$ are free to assume cis or trans configuration.

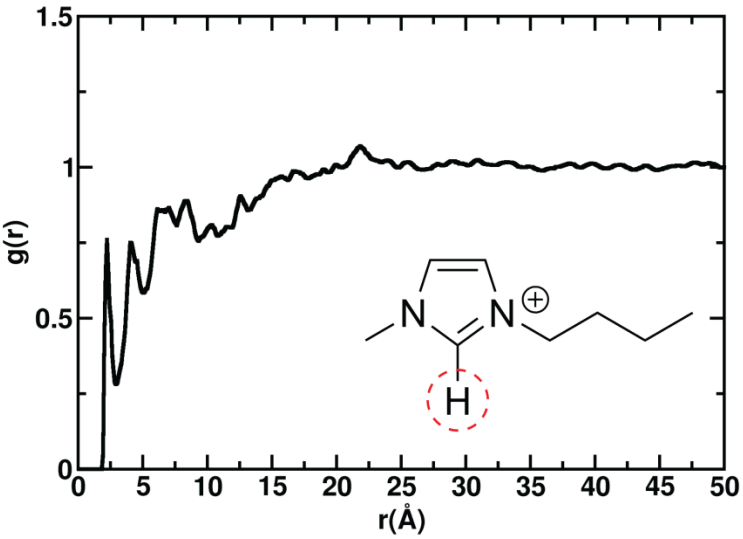

Fig. S6. Interaction of the H atom at the C(2) position of the $[bmim]^+$ cation (identified in the inset) with N of the h-BN sheet (Model 1). A sharp peak is observed at 2.24 Å, consistent with weak hydrogen bonding and in line with the notion that $[bmim]^+$ cations in $[bmim][NTf_2]$ orient themselves in a manner non-parallel with the BN surface. Despite the relatively weak hydrogen bond interactions between the cation and the h-BN sheets, these forces likely contribute partway to the putative exfoliation and dispersion of h-BN in this IL.

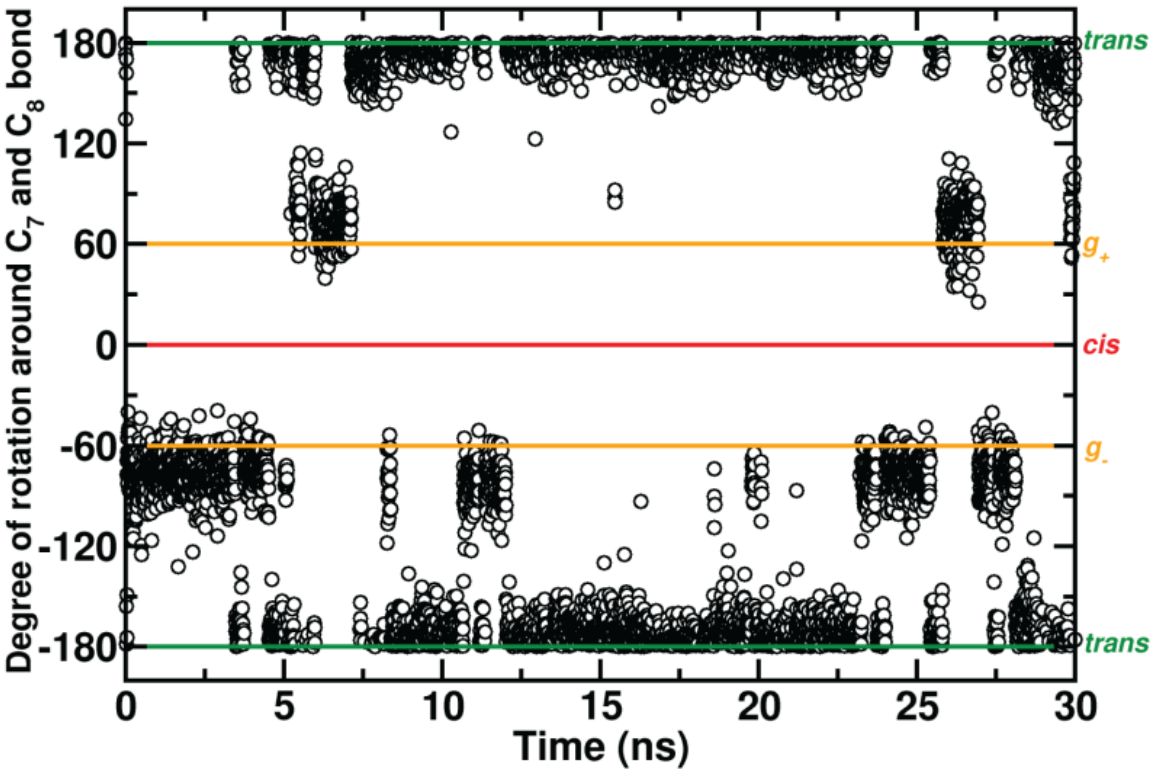

Fig. S7. The dihedral angle describing rotation about the C_7–C_8 bond in the butyl chain of $[bmim]^+$ interacting with the h-BN surface as the simulation proceeds. The butyl chain generally assumes a *trans* configuration but there exists a small energy barrier to rotation around this center bond, resulting in speedy interconversion between the $<g^+>$ and $<g^->$ gauche configurations. The C_7–C_8 bond of $[bmim]^+$ is defined in accordance with Fig. S4.

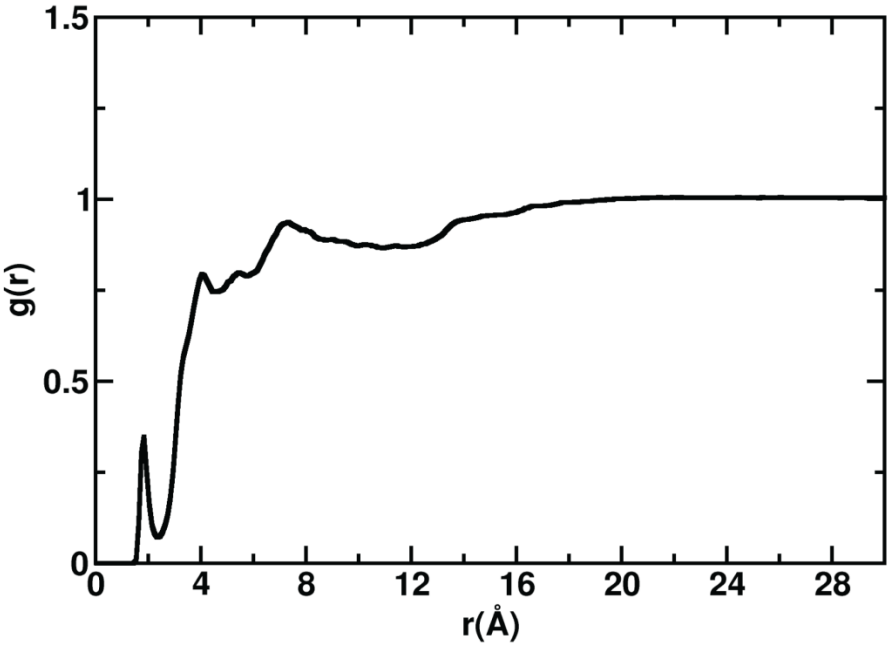

Fig. S8. Interaction of the H atoms in water with N of the h-BN sheet (Model 1). A weak peak around 1.85 Å suggests that H in water interacts weakly with N and may originate in the weak, experimentally-observed stabilization afforded to h-BN sheets in water. A full analysis of hydrogen bond dynamics throughout the entire 30-ns trajectory suggests that within the first solvation shell (4 Å) about 28% of the 339 water molecules form hydrogen bonds of various time fractions with nitrogen on the h-BN surface, of which less than 35% of this subset of water molecules engage in hydrogen bonds with greater than 50% occupancy over the entire simulation. This suggests that although not the dominant interaction, hydrogen bonding may nonetheless play a non-trivial role in water being a feasible medium for h-BN exfoliation.

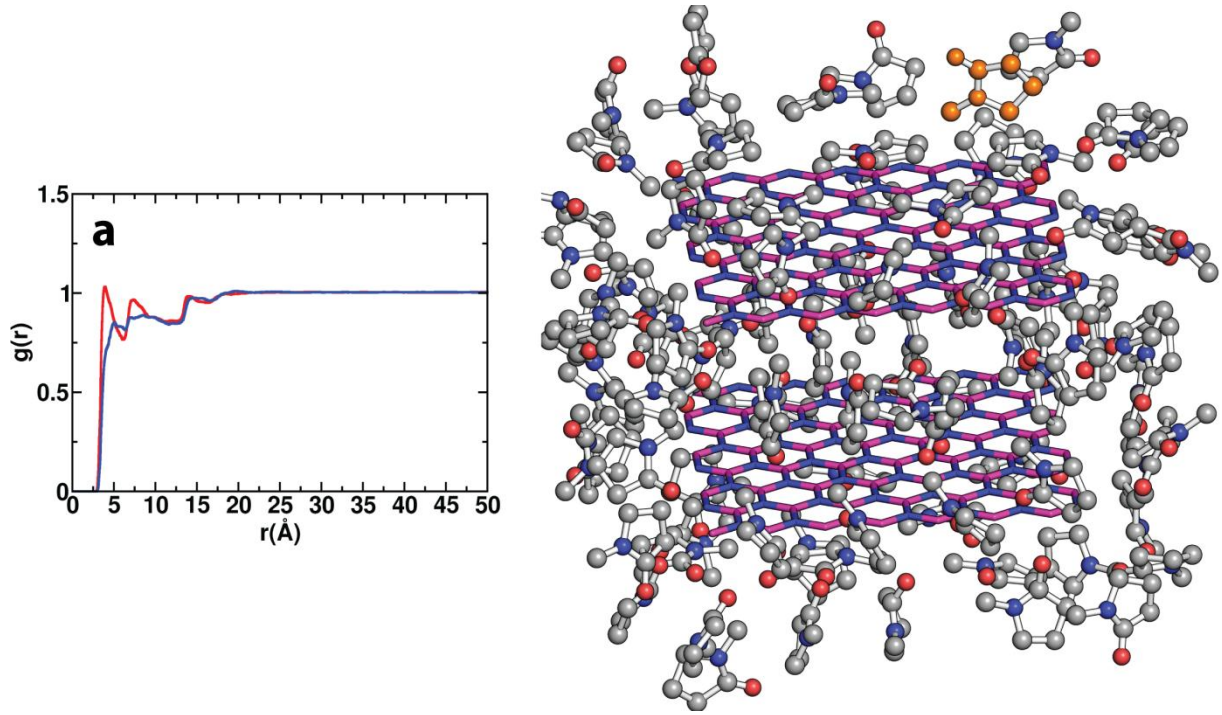

Fig. S9. NMP interactions with h-BN (Model 1). The left panel shows the RDFs of the methyl carbon (red curve) and ring (blue curve) of NMP with the h-BN surface. It can be seen that methyl interactions tend to dominate over ring interactions in a manner that parallels the interactions of $[Pyrr_{14}][NTf_2]$ with h-BN.

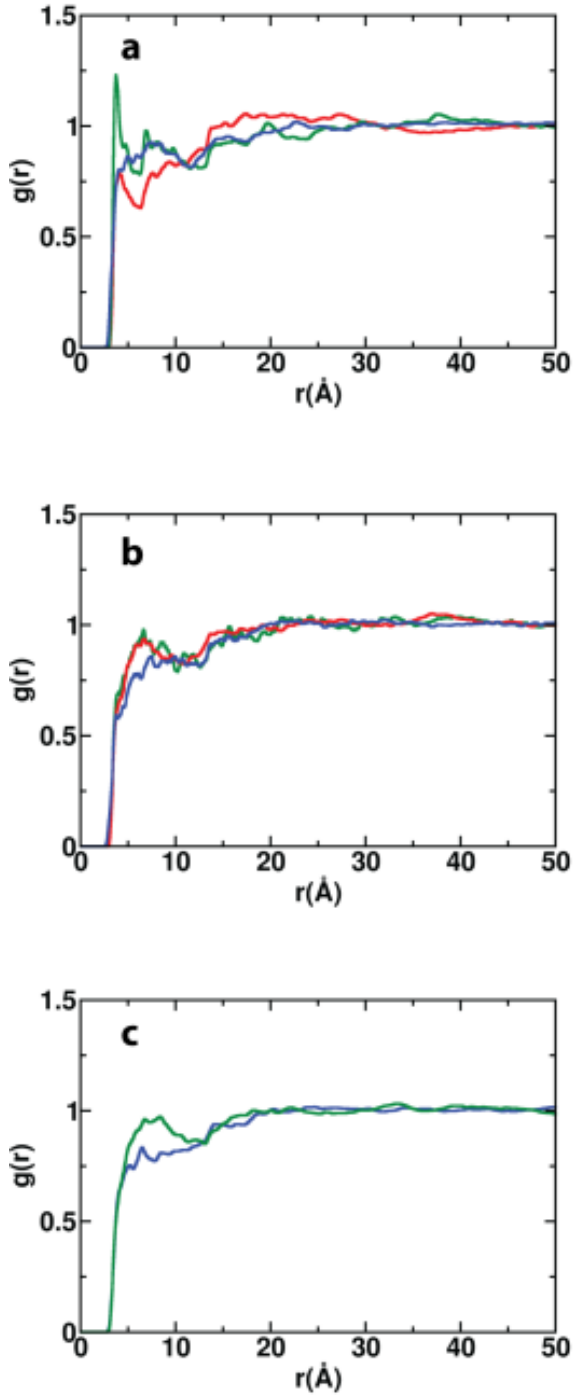

Fig. S10 IL cation interactions with h-BN according to Model 2: (a) $[bmim]^+$, (b) $[Pyrr_{14}]^+$, and (c) $[C_4Py]^+$. RDFs describing methyl carbon (red curve), butyl group (green), and ring center of mass (blue) interactions between the IL cation and the h-BN surface.

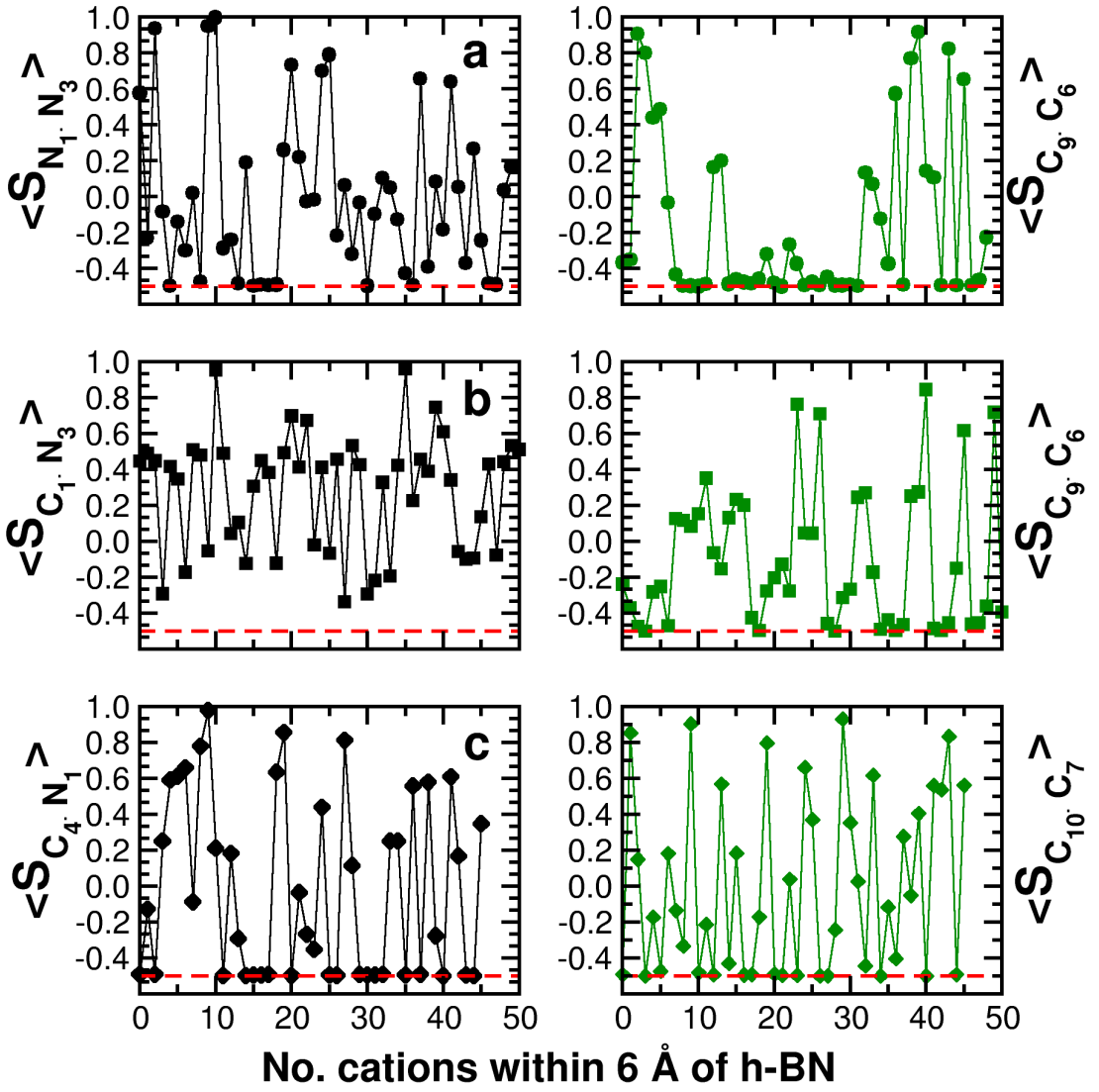

Fig. S11 Left panel: Order parameters of a) $[bmim]^+$, b) $[Pyrr_{14}]^+$, and c) $[C_4Py]^+$ cations within 6 Å of the h-BN sheets calculated via Model 2. Right panel: order parameters for the butyl chain vector for the corresponding cations according to Model 2. See Fig. S4 for the definition of the ordering parameters <S> for the cation and the butyl chain. The dashed red line indicates <S> = –0.5, indicating that the cation ring or the butyl chain is co-planar with the h-BN surface.

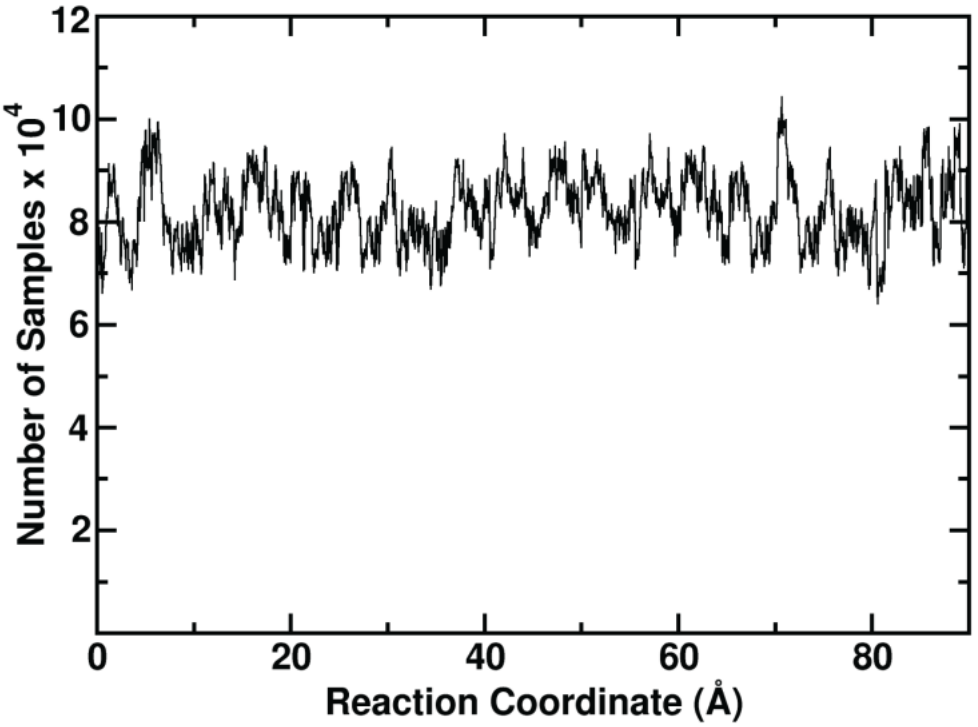

Fig. S12. Distribution of samples along the reaction coordinate for a 30 ns ABF–MD simulation describing an exfoliation process involving the transfer of an individual h-BN sheet initially paired to another h-BN sheet in a bilayered configuration solvated in [bmim][NTf_2] to isolation in vacuum.

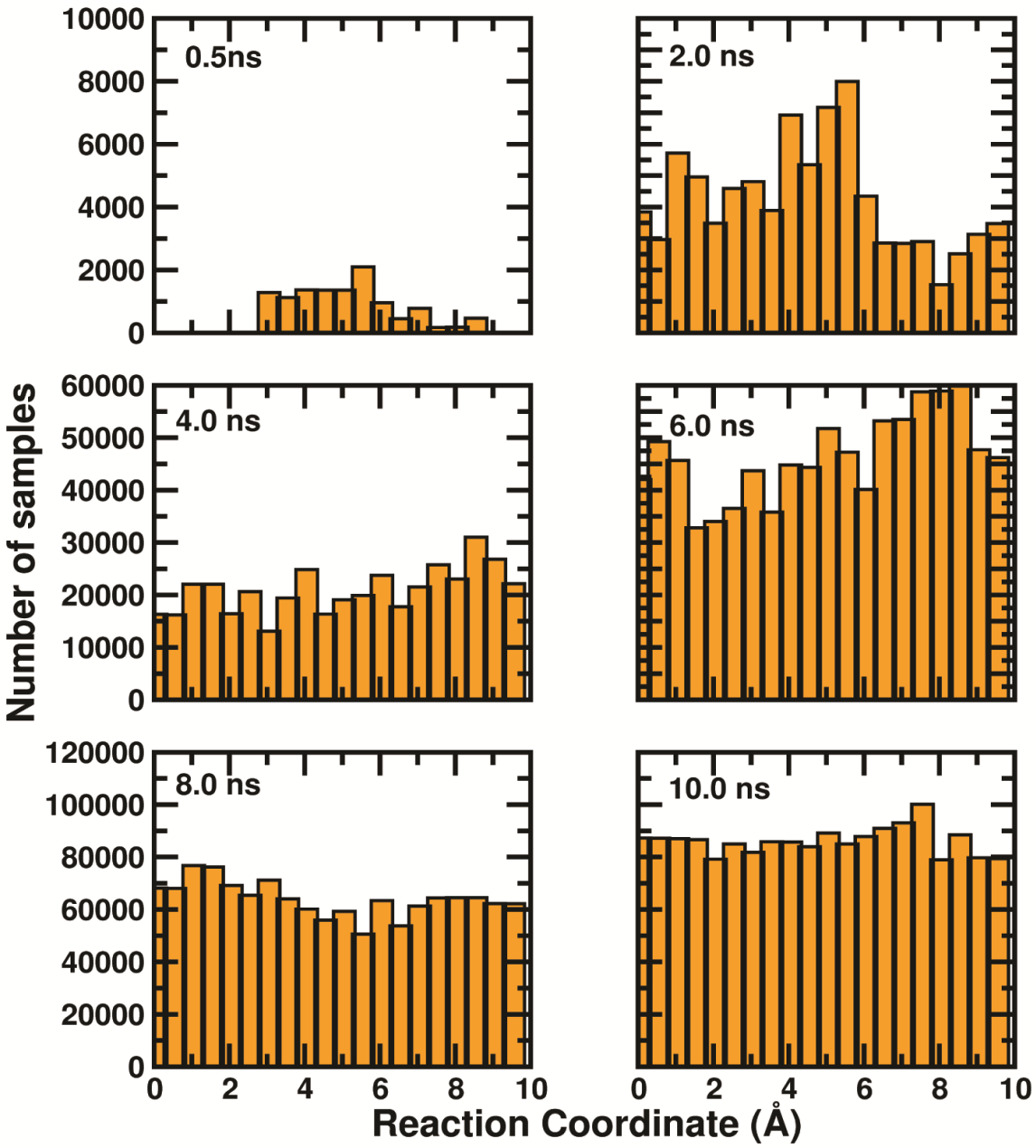

Fig. S13. Evolution in the sampling histograms generated from ABF–MD simulations conducted for 0.5, 2, 4, 6, 8, and 10 ns. These data confirm that, after 10 ns of simulation, the conformational phase space has been uniformly visited, verifying that the simulation has converged. Constraints are removed after the force is applied, so that the h-BN sheet can sample the conformational space and the high uniformity of sampling yields better statistics in the determination of the free energy.

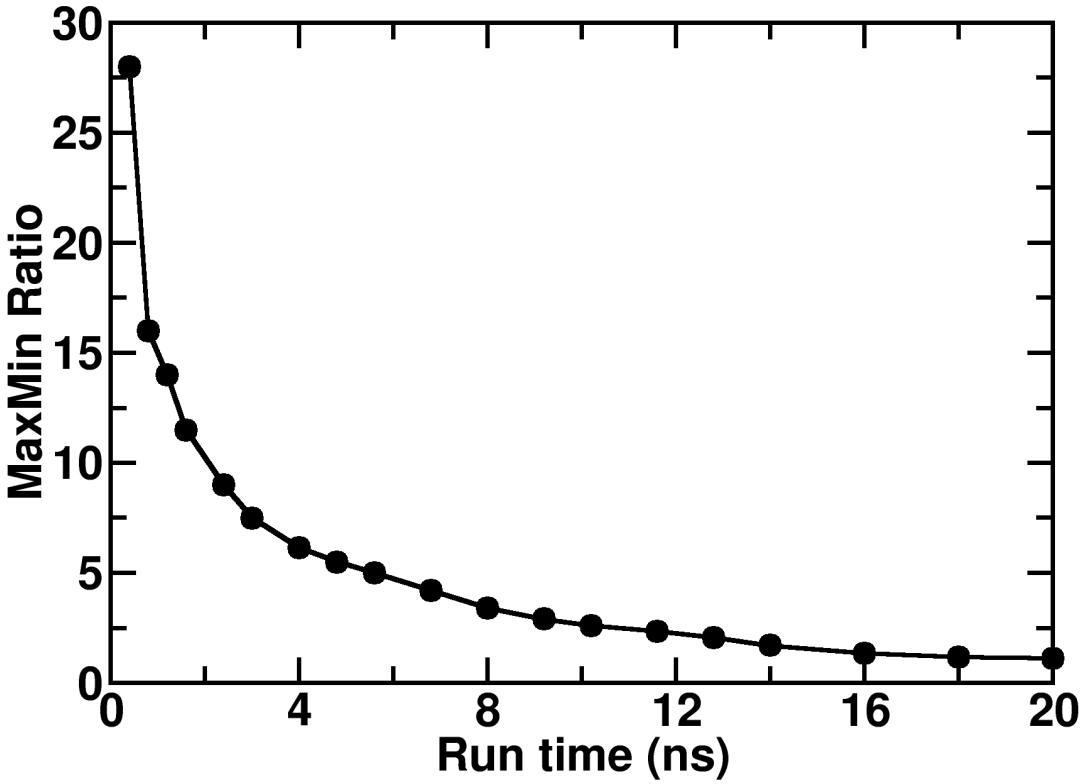

Fig. S14. Evolution of the MaxMin ratio for single h-BN sheet exfoliation from an original bilayer in [bmim][NTf_2] to vacuum during a representative 30 ns ABF–MD simulation run.

Methods

Adaptive biasing force (ABF) method is a technique developed by Darve et al. [S2] to calculate the free energy difference of certain chemical or biological processes along generalized reaction coordinates in the system of interest. This method is a combination of probability density and constraint force methods, and is based on the thermodynamic integration of average force acting on coordinates, which is unconstrained.[S2a] As a part of ABF algorithm, an external biasing force, estimated locally from the sampled conformations of the system and updated continuously, is applied at each step to facilitate the system in overcoming significant energy barriers along the reaction coordinate. This allows the system to evolve freely without constraints, enabling the simulation to visit multiple states separated by high free energy barriers and improving sampling long the reaction coordinate. A unique feature of the ABF method is the use of unconstrained reaction coordinates, thereby enabling unbiased and uniform sampling of the defined region.The theoretical foundation of this method is based on Eqn. 1, which is a modified version of the expression proposed by Darve and Pohorille[S2a, b] for the effective force (F^u) acting on the reaction coordinate (ξ),

$$F_{\xi}^{u} = m_{\xi}\frac{d^2\xi}{dt^2} + \frac{1}{\beta}\sum_{k=1}^{3M}\frac{1}{m_k}\frac{d\xi}{dx_k}\frac{dm_{\xi}}{dx_k} \quad (1)$$

where m_k are generalized masses associated with generalized coordinates represented by x_k.

The average of this applied force is equal and opposite to the mean force acting on ξ and cancels the free energy derivative computed for small intervals of reaction coordinate ξ so that the system can evolve and overcome free energy barriers.

$$\langle\frac{\partial H}{\partial \xi}\rangle_{\xi} = -\langle F_{\xi}^{u}\rangle_{\xi} \quad (2)$$

The Helmholtz free energy A at constant temperature T, constant volume V and number of particles N is given by:

$$A(N,V,T) = -k_b T \log Z(N,V,T) \quad (3)$$

where Z is the canonical partition function and k_b is the Boltzmann's constant.

The free energy as a function of the reaction coordinate can be written as:

$$A(N,V,T,\xi) = -k_b T \log \frac{\int \exp[-\beta H(x,p)]\delta(\xi(x)-\xi_o)dx\,dp}{\Lambda^{3M} N!} \quad (4)$$

where Λ is the thermal wavelength and *p* is the conjugate momenta of position coordinate *x*.

It is more convenient to compute the free energy difference $\Delta \boldsymbol{A}_{\boldsymbol{a}\rightarrow\boldsymbol{b}}$ between state A and B for a system. The states A and B are based on the reaction coordinate which is a function of the particle position.

$$\Delta \boldsymbol{A}_{\boldsymbol{a}\rightarrow\boldsymbol{b}} = \int_{\xi_a}^{\xi_b} \frac{\boldsymbol{dA}(\boldsymbol{\xi})}{\boldsymbol{d\xi}}\, \boldsymbol{d\xi} \qquad \textbf{(5)}$$

The first derivative of the free energy is related to the partial derivative of the Hamiltonian of the system with the reaction coordinate[S3] and therefore based on Eqn. **5** can be related to the constraint force acting along the reaction coordinate

$$\Delta \boldsymbol{A}_{\boldsymbol{a}\rightarrow\boldsymbol{b}} = \int_{\xi_a}^{\xi_b} \frac{\boldsymbol{dA}(\boldsymbol{\xi})}{\boldsymbol{d\xi}}\, \boldsymbol{d\xi} = \int_{\xi_a}^{\xi_b} \langle \frac{\boldsymbol{dH}(\boldsymbol{\xi})}{\boldsymbol{d\xi}} \rangle_{\xi}\, \boldsymbol{d\xi} = \int_{\xi_a}^{\xi_b} -\langle \boldsymbol{F}_{\boldsymbol{\xi}}^{\boldsymbol{u}} \rangle_{\xi}\, \boldsymbol{d\xi} \qquad \textbf{(6)}$$

Further details of the ABF method and formulation including the implementation in NAMD[4] molecular dynamics package can be found in these publications.[S2-3, 5] The Helmholtz free energy ***A*** obtained from NVT ensemble simulations is in close approximation to the Gibbs free energy ***G*** in condensed phase.[S6] The Gibbs free energy difference is used to compute the free energy of hydration and partition function.

Intermolecular Potential

The force field developed by Lopes and co-workers based on the OPLS/AMBER framework was used to model the dialkylimidazolium,[S7] N-butylpyridinium, [S8] cation and anion [NTf_2]. [S9] This force field for ionic liquids is based on the 12-6 Lennard Jones model and unity point charges and predicts the pure component thermodynamic properties in good agreement with experiment. The force field for h-BN sheet was based on the parameters from Won and Aluru. [S10] The force field is also based on the 12-6 potential, therefore making it easy to use the combining rules for non–bonded interactions of h-BN with IL, NMP or water. The R_{min} of the boron is set at 1.93 Å and the well depth of the boron is 0.0949 kcal mol^{-1} with q charge of 1.05, while the R_{min} of the nitrogen is 1.88 Å and the well depth of the nitrogen is 0.145 kcal mol^{-1} with charge of –1.05. The boron–nitrogen equilibrium bond length was 1.446 Å with the stretching force constant set at 322.55 kcal mol^{-1}, angle bending force constant at 53.35 kcal mol^{-1} and torsional force constant at 3.15 kcal mol^{-1}.

Simulation Details

In this work the adaptive force bias method[2a] adopted in NAMD version 2.7b3[5c] is used to determine the free energies of exfoliation of h-BN from a "bilayer" using three cations based bis(trifluoromethanesulfonyl)imide (NTf_2) anion ILs. As a part of ABF algorithm, an external biasing force, estimated locally from the sampled conformations of the system and updated continuously, is applied at each step to facilitate the system in overcoming significant energy barriers if present along the reaction coordinate. This force is applied to one layer of the h-BN sheet in tangential *z* direction with respect to the other layer. This mimics the shearing force provided by the solvent media for exfoliation of h-BN monolayers from the bilayer. The h-BN

sheets were separated by 10 Å. This separation was chosen so that the IL could fill in the space during MD equilibration. The h-BN layers are allowed to evolve freely without any constraints enabling the simulation to visit multiple states separated by high energy barriers resulting in an improved sampling of the reaction coordinate. For all systems, a rectangular simulation cell was used, with dimensions 80 Å × 80 Å × 200 Å, with the condensed phase occupying a region 80 Å × 80 Å × 80 Å. The number of molecules in each box was selected to reproduce the densities of the different ILs predicted by isothermal–isobaric (NPT) simulations at 1 atm and 300 K for a specific potential truncation (14 Å). For systems utilizing a 14 Å cut–off, 1200 IL molecules were used, respectively. Initial configurations for each system were generated with Packmol followed by minimization and MD using NAMD. Energy minimization was performed on all systems for 500 steps using the steepest descent technique. Systems were equilibrated over a time period of 10 ns in isobaric–isothermal ensemble at 1.0 atm and 300 K, with another production of 20 ns, followed by the ABF calculation in the isothermal NVT ensemble for 30 ns for each window.

A rectangular simulation cell was used, with dimensions 80 Å × 80 Å × 200 Å, with the condensed phase occupying a region approximately 80 Å × 80 Å × 80 Å. This cell was extended to 200 Å in the z–direction with a 120 Å vacuum region. The vacuum region is necessary to prevent interactions of the solute with the condensed phases through periodic boundary conditions. The number of molecules in each box was selected to reproduce the density of the ionic liquid as predicted by *NPT* simulations at 1 atm and 300 K for a specific potential truncation (14 Å). The reaction coordinate for the determination of free energy changes was defined as the distance between the center of mass of the h-BN sheet (COMS) under study and center of mass of the condensed phase (COMCP). In the initial system setup, the COMS was placed at approximately the COMCP. Over the course of simulation, the reaction coordinate spanned a distance of 120.0 Å from the center of mass of the condensed phase to the center of the vacuum region. To reduce the statistical error of the calculations, the reaction pathway was divided into nine equally sized non–overlapping windows of 10.0 Å. To generate the initial configurations for each window, a single 30 ns ABF run was performed spanning the complete reaction pathway from 0.0 Å to 90.0 Å after heating and equilibration of the system. Coordinates from the trajectory of this simulation were saved periodically to generate nine initial coordinate files for the nine windows. Force statistics were stored in bins of width 0.05 Å. The biasing force was applied after 500 samples were collected in each bin. To keep the solute within the specified window, a harmonic force with a magnitude of 10.0 kcal mol^{-1} $Å^{-1}$ was applied on the upper and lower boundary of the window along the *z*-axis of the simulation cell. A final production run of 30 ns for each window was performed.

Molecular dynamics simulations were performed with NAMD version 2.7b3.[S4] Initial configurations for each system were generated with Packmol.[S11] Energy minimization was performed on all systems for 500 steps using the steepest decent technique. Systems were equilibrated over a time period of 10.0 ns in isobaric–isothermal ensemble at 1.0 atm and 300 K, followed by production time of 30.0 ns, subsequently followed by ABF–MD calculation in NVT ensemble. For all calculations, the temperature was maintained at 300 K using Langevin dynamics. For initial *NPT* simulations, used to determine the density of each system, constant pressure was maintained at 1.0 atm using the Nose–Hoover algorithm.[S12, S13] A timestep of 1.0 fs was used for the integration of Newton's equation of motion. Periodic boundary conditions were used in all the three spatial coordinates. Long range electrostatic interactions were calculated with particle–mesh Ewald algorithm.[S14] A switching function was applied for all Lennard–Jones

interactions at 12.5 Å for 14.0 Å cut-off. Data were analysed using VMD.[S15]

Convergence of the ABF–MD

To validate the sampling behaviour of our ABF–MD simulations for the systems used in this study, a test case of h-BN monolayer transfer from an initial bilayer construct in [bmim][NTf_2] to vacuum was chosen for which the number of samples accumulated at the end of the simulation were plotted as a function of reaction coordinate. Plots generated in this manner (Fig. S12) suggest uniform sampling for the complete reaction pathway. Evolution of sampling was also studied for the above test case. Sampling histograms were generated at various intervals during the course of simulation as a function of the reaction coordinate. By 0.5 ns, only a few locations were sampled while the others remain unvisited. As time proceeded, the sampling became uniform and attained uniformity around 10 ns, indicating the convergence of ABF run (Fig. S13). The MaxMin ratio, the ratio of maximum to minimum number of samples collected in a specific region along the reaction coordinate is essentially infinite at 0.5 ns but drops to 1.16 after 16 ns of run time. This confirms that all locations have been visited for an equivalent number of times, marking the convergence of the ABF run (Fig. S14) and free energy predictions.

Surface Tension of the Liquid-Vacuum Interface

Interfacial properties were calculated from simulations using orthorhombic cells with lengths such that X ~ Y < Z, according to the fact that the interface is oriented perpendicularly to the *z* direction. For the determination of surface tension, a slab of ionic liquid, consisting of 1280 ion pairs, is sandwiched between two vacuum regions. The entire simulation cell has dimensions of 720 Å × 770 Å × 500 Å. These values and protocol were based on work from Merlet and co-workers [S16] for estimation of the surface tension of their coarse grained models for [emim][BF_4]. Three sets of independent simulations were performed for the three ILs studied in this work at 300 K, and allowed to relax for 10 ns in the NVT ensemble. The statistics are then gathered for the next 10 ns using the same conditions. The surface tension was estimated from the pressure tensor values *P* obtained from the simulations.

$$\gamma = \frac{Z}{2}\left(\langle P_{zz}\rangle - \left\langle \frac{P_{xx}+P_{yy}}{2}\right\rangle\right) \qquad (7)$$

The computed surface tension for [bmim][NTf_2] was 42.3±0.8 mN/m at 300 K in comparison to the experimental value of 33.23 mN/m at 298 K. [S17] Similarly, the surface tension computed for [C_4Py][NTf_2] was overpredicted. In this case, the model estimation was 43.4±0.6 mN/m at 300 K in comparison to an experimental value of ~33.3 mN/m (33.4 mN/m at 298.15 K and 33.2 mN/m at 303.15 K).[S18] Finally, for [Pyrr][NTf_2], the model predicts a surface tension of 41.7±0.9 mN/m at 300 K. While these computed surface tensions are overpredicted in comparison to experiment, they fall in agreement with previous simulation results for ILs using the Lopez and Padua force field, which revealed that the surface tension values were overpredicted for other ILs. [S19] [S20] Nevertheless, these results remain in solidarity with the hypothesis that solvents with a surface tension in the vicinity of 40 mJ m^{-2}, roughly matched to the surface energy of BN powder (47–63 mJ m^{-2}), should offer effective media for producing 2-D h-BN nanosheets from the layered material. It follows that, with surface tensions for typical ILs ranging from about 33

to 45 mJ m^{-2}, it might reasonably be anticipated that ILs represent beneficial and fascinating media for creating nanosheets from bulk h-BN in a liquid exfoliation process. Our computational results are certainly in line with this scenario.

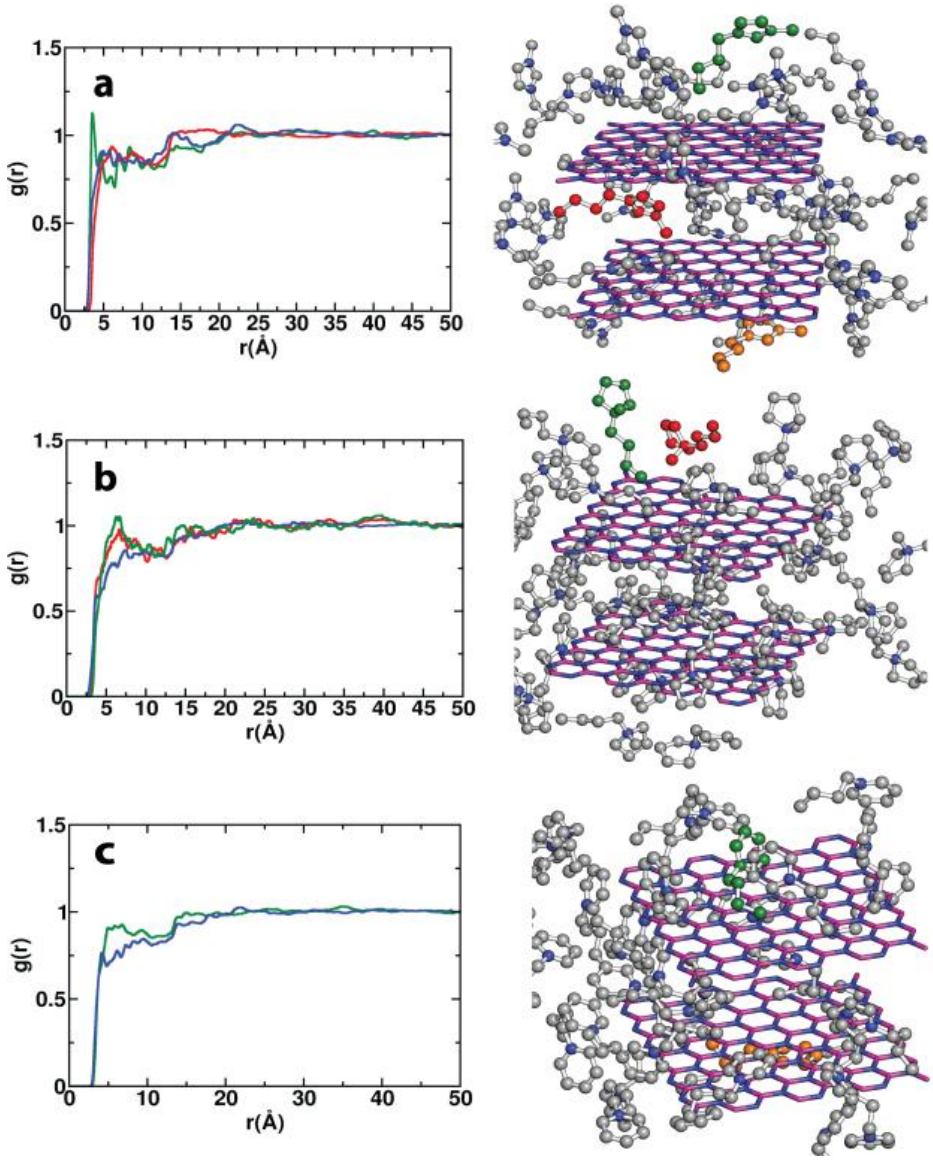

Fig. S15 IL cation interactions with h-BN: (a) $[bmim]^+$, (b) $[Pyrr_{14}]^+$, and (c) $[C_4Py]^+$. (Left) Radial distribution functions describing methyl carbon (red curve), butyl group (green), and ring center of mass (blue) interactions between the IL cation and the h-BN surface. *Note:* These profiles are identical to those presented in Fig. 2 except that the long-range interactions up to 50 Å are also shown. (Right) Simulation snapshots showing representative interactions occurring between the methyl carbon (orange), butyl chain (green), and ring (red) of the corresponding cations and the h-BN surface. The hydrogens have been omitted for visual clarity, the carbon atoms of the IL cations are shown in grey, and nitrogens are blue.

References

S1. Lisal, M.; Posel, Z.; Izak, P. Air-Liquid Interfaces of Imidazolium-Based Ionic Liquids: Insights from Molecular Dynamics Simulations. *Phys. Chem. Chem. Phys.* **2012**, *14*, 5164.
S2. (a) Darve, E.; Pohorille, A. Calculating Free Energies Using Average Force. *J. Chem Phys* **2001**, *115*, 9169; (b) Darve, E.; Wilson, M. A.; Pohorille, A. Calculating Free Energies Using a Scaled-Force Molecular Dynamics Algorithm. *Mol. Simulat.* **2002**, *28*, 113; (c) Rodriguez-Gomeza, D.; Darveb, E.; Pohorille, A. Assessing the Efficiency of Free Energy Calculation Methods. *J. Chem. Phys.* **2004**, *120*, 3563.
S3. Darve, E.; David Rodríguez-Gómez; Pohorille, A. Adaptive Biasing Force Method for Scalar and Vector Free Energy Calculations. *J. Chem. Phys.* **2008**, *128*, 144120.
S4. Phillips, J. C.; Braun, R.; Wang, W.; Gumbart, J.; Tajkhorshid, E.; Villa, E.; Chipot, C.; Skeel, R. D.; Kale, L.; Schulten, K. Scalable Molecular Dynamics with NAMD. *J. Comp. Chem.* **2005**, *26*, 1781.
S5. (a) Chipot, C.; Hénin, J. Exploring the Free-Energy Landscape of a Short Peptide Using an Average Force. *J. Chem. Phys.* **2005**, *123*, 244906. (b) Hénin, J.; Chipot, C. Overcoming Free Energy Barriers Using Unconstrained Molecular Dynamics Simulations. *J. Chem. Phys.* **2004**, *121*, 2904; (c) Hénin, J.; Fiorin, G.; Chipot, C.; Klein, M. L. Exploring Multidimensional Free Energy Landscapes Using Time-Dependent Biases on Collective Variables. *J. Chem. Theo. Comput.* **2010**, *6*, 35; (d) Chipot, C.; Pohorille, A., *Free Energy Calculations: Theory and Applications in Chemistry and Biology*, Springer Series in Chemical Physics; Springer: 2007.
S6. Buhl, M.; Wipff, G. Insights into Uranyl Chemistry from Molecular Dynamics Simulations. *ChemPhysChem* **2011**, *12*, 3095.
S7. (a) Lopes, J.; Deschamps, J.; Padua, A. Modeling Ionic Liquids Using a Systematic All-Atom Force Field. *J. Phys. Chem. B* **2004**, *108*, 2038; (b) Lopes, J. N. C.; Deschamps, J.; Padua, A. A. H. Modeling Ionic Liquids Using a Systematic All-Atom Force Field. Addition/Correction. *J. Phys. Chem. B* **2004**, *108*, 11250.
S8. Lopes, J. N. C.; Padua, A. l. A. H. Molecular Force Field for Ionic Liquids III: Imidazolium, Pyridinium, and Phosphonium Cations; Chloride, Bromide, and Dicyanamide Anions. *J. Phys. Chem. B* **2006**, *110*, 19586.
S9. (a) Lopes, J. N. C.; Padua, A. l. A. H. Molecular Force Field for Ionic Liquids Composed of Triflate or Bistriflylimide Anions. *J. Phys. Chem. B* **2004**, *108*, 16893; (b) Shimizu, K.; Almantariotis, D.; Margarida F. Costa Gomes; Padua, A. l. A. H.; Lopes, J. N. C. Molecular Force Field for Ionic Liquids V: Hydroxyethylimidazolium, Dimethoxy-2-Methylimidazolium, and Fluoroalkylimidazolium Cations and Bis(Fluorosulfonyl)Amide, Perfluoroalkanesulfonylamide, and Fluoroalkylfluorophosphate Anions. *J. Phys. Chem. B* **2010**, *114*, 3592.
S10. Won, C. Y.; Aluru, N. R. Water Permeation through a Subnanometer Boron Nitride Nanotube. *J. Am. Chem. Soc.* **2007**, *129*, 2748.
S11. Martinez, L.; Andrade, R.; Birgin, E. G.; Martinez, J. M. Packmol: A Package for Building Initial Configurations for Molecular Dynamics Simulations. *J. Comput. Chem.* **2009**, *30*, 2157.
S12. Feller, S. E.; Zhang, Y. H.; Pastor, R. W.; Brooks, B. R. Constant-Pressure Molecular-Dynamics Simulation - the Langevin Piston Method. *J. Chem. Phys.* **1995**, *103*, 4613.
S13. Martyna, G. J.; Tobias, D. J.; Klein, M. L. *J. Chem . Phys.* **1994**, *101*, 4177.
S14. (a) Darden, T.; York, D.; Pedersen, L. Particle Mesh Ewald: an $N\cdot\mathrm{Log}(N)$ Method for Ewald Sums in Large Systems. *J. Chem. Phys.* **1993**, *98*, 10089; (b) Essmann, U.; Perera, L.;

Berkowitz, M. L.; Darden, T.; Lee, H.; Pedersen, L. G. A Smooth Particle Mesh Ewald Method. *J. Chem. Phys.* **1995**, *103*, 8577.
S15. Humphrey, W.; Dalke, A.; Schulten, K. VMD: Visual Molecular Dynamics. *J. Mol. Graphics* **1996**, *14*, 33.
S16. Merlet, C.; Salanne, M.; Rotenberg, B. New Coarse-Grained Models of Imidazolium Ionic Liquids for Bulk and Interfacial Molecular Simulations. *J. Phys. Chem. C* **2012**, *116*, 7687.
S17. Tariq, M.; Freire, M. G.; Saramago, B.; Coutinho, J. A. P.; Lopes, J. N. C.; Rebelo, L. P. N. Surface Tension of Ionic Liquids and Ionic Liquid Solutions. *Chem. Soc. Rev.* **2012**, *41*, 829.
S18. Liu, Q.-S.; Yang, M.; Yan, P.-F.; Liu, X.-M.; Tan, Z.-C.; Welz-Biermann, U. Density and Surface Tension of Ionic Liquids [Cnpy][NTf2] (N = 2, 4, 5). *J. Chem. Eng. Data* **2010**, *55*, 4928.
S19. Merlet, C. l.; Salanne, M.; Rotenberg, B.; Madden, P. A. Imidazolium Ionic Liquid Interfaces with Vapor and Graphite: Interfacial Tension and Capacitance from Coarse-Grained Molecular Simulations. *J. Phys. Chem. C* **2011**, *115*, 16613.
S20. Bhargava, B. L.; Balasubramanian, S. Layering at an Ionic Liquid−Vapor Interface: A Molecular Dynamics Simulation Study of [Bmim][PF_6]. *J Am. Chem. Soc.* **2006**, *128*, 10073.